Relaxation of a rubbed polystyrene surface

Alexander D. Schwab and Ali Dhinojwala*
Department of Polymer Science, The University of Akron, Akron, Ohio 44325
(Received 9 August 2002; revised manuscript received 25 November 2002; published 10 February 2003)

The relaxation dynamics of a rubbed polystyrene (PS) surface have been characterized using infrared-visible sum frequency generation spectroscopy (SFG). The SFG results were compared with previous relaxation of retardation measurements, and the results show that the rubbed PS surface has the same T_g as the bulk where T_g is defined as $\tau(T_g)=5$ s, however, the surface has a lower activation energy (ΔE) and a larger stretching exponent (β_{KWW}) than bulk PS. This indicates that the surface region relaxes more quickly than the bulk. The thickness of this region of lower ΔE and larger β_{KWW} is estimated to be roughly 12 nm.

DOI: 10.1103/PhysRevE.67.021802 PACS number(s): 36.20.−r, 61.20.Lc, 64.70.Pf, 68.15.+e

I. INTRODUCTION

The glass transition temperature (T_g) of thin supported polymer films has been the subject of intense experimental study over the past few years. Measurements of the average T_g of atactic polystyrene (PS) films on nonattractive substrates reveal that film T_g drops up to 30 K with decreasing film thickness [1–7]. Several authors hypothesize on the existence of a layer with enhanced mobility at the free surface of the film and that this layer of enhanced mobility dominates the overall film properties as the film thickness decreases [1–7]. Attempts have been made to measure the dynamic properties of PS free surfaces with conflicting results. Dynamic atomic force microscope measurements of a PS free surface find either no change in the surface T_g [8] or a significant decrease in the surface T_g [9] relative to bulk PS. Near edge x-ray absorption fine structure (NEXAFS) measurements on oriented PS surfaces reveal no enhancement [10] or significant enhancement [11] of the surface relaxation dynamics relative to the bulk. Finally, positron annihilation lifetime spectroscopy measurements of the PS free surface indicate the surface has the same T_g [12] and a T_g 57 K lower than the bulk [13].

To better quantify relaxation dynamics at the PS-air interface, we have measured the relaxation of rubbing induced orientation of PS phenyl side groups using an inherently surface sensitive technique, infrared-visible sum frequency generation spectroscopy (SFG). In SFG, the system to be studied is exposed to a high-intensity visible laser beam (800 nm) and a tunable infrared laser beam (2750–3150 cm^{-1}). Based upon a dipole approximation, a group of molecules will emit no net SFG if the molecular dipoles are centrosymmetric, as is the case in an amorphous polymer glass such as PS. At the PS film interfaces, however, this centrosymmetry is broken; therefore SFG is generated only by the surface.

The surface relaxation data obtained from SFG are also compared with previous results obtained for near-surface relaxations in rubbed PS probed with optical retardation measurements [6,7]. This study shows that the surface has the same T_g as the bulk, but the temperature dependence of the surface relaxation times below T_g has a lower activation energy than in the bulk. Simply stated, at any temperature below T_g, a surface region ~12-nm thick relaxes more quickly than the bulk.

II. EXPERIMENT

A. SFG measurements

The visible and tunable IR laser beams have a pulse width of 1 ps and a repetition rate of 1 kHz and are produced by a Spectra Physics Spitfire and OPA-800, respectively. The average visible and IR intensities are 200 mW and 1–2 mW, respectively, and the resulting IR pulse energy is well described by a Gaussian probability distribution with a standard deviation of 8.7 cm^{-1}. SFG signals from sample interfaces are passed through optical notch filters and detected using a photomultiplier tube with gated photon counting electronics. SFG signals are normalized to the average IR intensity obtained by taking a fraction of the IR beam to a pyroelectric detector.

B. Birefringence measurements

The optical train for the birefringence measurements was composed of a HeNe laser light source, a polarizer oriented at +45°, a photoelastic modulator (PEM), the sample to be studied mounted on a rotation stage, a polarizer oriented at −45°, and finally a Si photodiode detector. The light intensity at the photodiode was measured at one and two times the modulation frequency of the PEM and the birefringence was obtained from these intensities [14].

C. Sample preparation

For all the measurements presented in this paper, PS ($M_n=62\,600$ g mol^{-1}, $M_w/M_n=1.03$) films were prepared by spin coating from toluene solution on substrates that were cleaned in a base bath, rinsed with deionized water, dried with N_2, and Ar plasma cleaned. The films were annealed 10–30 K above bulk T_g for at least 2 h and cooled slowly to room temperature under vacuum. The substrates used depended on the experimental technique used and the type of experiment. Thin glass microscope cover slides, glass microscope slides, and sapphire prisms were used as substrates for birefringence measurements, measurements of the in-plane

*Corresponding author.

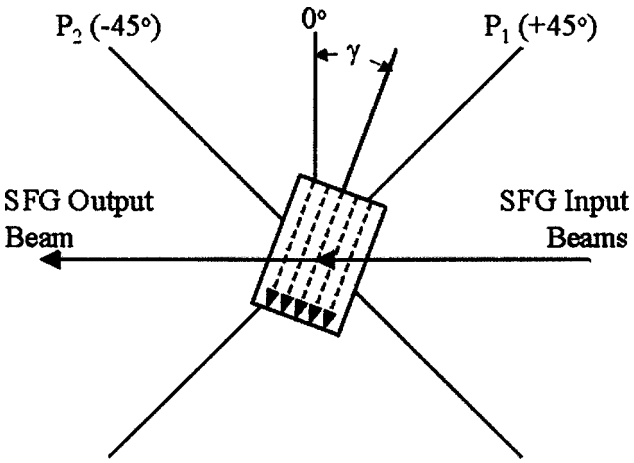

FIG. 1. Diagram relating the orientation of the sample relative to the polarizer (P_1) and analyzer (P_2) of the birefringence measurement apparatus as well as to the incident and output beams of the SFG experiment. The rubbing direction on the PS film, indicated by the dashed arrows, is rotated an angle γ with respect to the vertical plane. This view is drawn looking at the sample surface from the side of the incident beams.

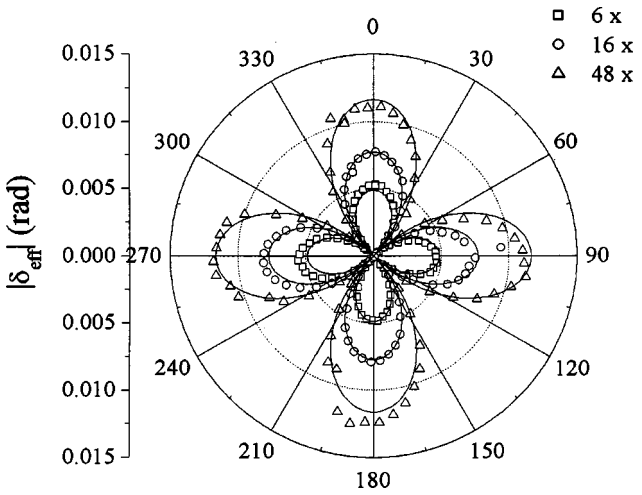

FIG. 2. Plot of effective retardation, δ_{eff} as a function of the rotation angle γ as seen in Fig. 1 for a (200 ± 10)-nm-thick PS film rubbed 6, 16, and 48 times with a velour cloth. The lobes at 0°, 90°, 180°, and 270° indicate that the optic axes of the sample are parallel to and perpendicular to the rubbing direction in the film. The relative size of the lobes indicates that the sample's retardation increases with the number of rubbing iterations.

anisotropy of SFG intensity caused by film rubbing, and relaxation of SFG intensity measurements, respectively. The sapphire prism allowed the use of a total internal reflection geometry that has been shown to give a significant enhancement in the SFG intensity when the incident angle is near the critical angle of total internal reflection [15].

III. RESULTS AND DISCUSSION

A. Static birefringence measurements

The birefringence instrument described in the experimental section measures the effective retardation of light caused by the sample as the sample is rotated about the surface normal by the angle γ shown in Fig. 1. The dependence of the effective retardation on the rotation angle can be determined by modeling the train of optical elements with Jones matrices [16]. The resulting expression for the relationship between the measured effective retardation δ_{eff}, the rotation angle γ, and the true sample retardation δ, is

$$|\delta_{\text{eff}}| = 2\sin^{-1}\left[\cos(2\gamma)\sin\left(\frac{\delta}{2}\right)\right]. \tag{1}$$

When δ_{eff} is measured over a wide range of rotation angles, the direction of the optic axes of the sample birefringence as well as the sign of the birefringence can be determined. When the sample is oriented with $\gamma = k90°$ $(k=0,1,2,3)$, Eq. (1) becomes $\delta_{\text{eff}}=\delta$ and the birefringence instrument then measures the retardation of the sample. The retardation δ represents the phase difference between light transmitted through the sample polarized in the directions of the sample's optic axes. The expression that relates the sample retardation to the birefringence in the sample is

$$\delta = \int_0^{-h} \frac{2\pi\Delta n(z)}{\lambda}\, dz, \tag{2}$$

where h is the film thickness and $\Delta n(z)$ is the birefringence at a distance z from the PS-air interface $(z=0)$. After application of some simplifying assumptions that are described later, the sample's retardation is the product of the birefringence in the sample, Δn, and the thickness over which this birefringence exists, d_{eff}:

$$\delta = \frac{2\pi\Delta n d_{\text{eff}}}{\lambda}, \tag{3}$$

where λ is the wavelength of light used (632.8 nm) [6,7,17].

The retardation of a PS film (200 ± 10)-nm-thick rubbed different amounts with a velour cloth and measured at different sample orientations (Fig. 1) can be found in Fig. 2. The birefringence measured by the instrument is at a maximum when $\gamma = k90°$ $(k=0,1,2,3)$, indicating that the sample's optic axes are parallel and perpendicular to the rubbing direction in the film. As the sample is rubbed an increasing number of times, the retardation of the film increases, and the optic axes remain parallel and perpendicular to the direction of rubbing, as seen by the increasing sizes of the effective retardation lobes in Fig. 2. We were also able to determine the absolute sign of the retardation by calibrating the instrument with a sample of known retardation. The rubbed PS film exhibits negative birefringence, meaning the refractive index of the sample increases perpendicular to the direction of rubbing. This same phenomenon is found for PS films uniaxially stretched at elevated temperatures and is attributed to the highly polarizable phenyl side groups becoming oriented perpendicular to the direction of stretching of the polymer backbone [18].

Upon inspection of Eqs. (2) and (3), it is apparently not possible to determine whether the increase in retardation with rubbing is due to an increase in the orientation (Δn) or an increase in the depth of the rubbing, d_{eff}. A study on

polyimide films of different thicknesses rubbed with varying rubbing strengths indicates that the birefringence of the oriented portion of the film is uniform to a certain depth and that this depth increases with rubbing strength; whereas the amount of orientation (Δn) is independent of rubbing strength [6,7,17]. It is based on these findings that Eq. (3) becomes valid. Therefore, the increase in retardation seen with rubbing iterations in Fig. 2 is due to the increased depth of orientation of PS chains rather than the increased magnitude of orientation.

B. Static SFG measurements

We have previously characterized both the PS-air and PS-substrate interfaces of a PS film on sapphire using SFG in the internal reflection geometry [15]. Phenyl C-H stretching vibrations, the most prominent at 3070 cm^{-1} corresponding to the ν_2 vibrational mode, dominate the SSP polarized (*s*-polarized SFG, *s*-polarized visible, and *p*-polarized infrared) SFG spectrum of the PS-air interface. This is indicative of a surface populated by phenyl side groups that are oriented nearly perpendicular to the surface of the film [15,19]. Spectra obtained using external reflection geometry and an incident angle of ~60° appear identical to spectra of the PS-air interface obtained using internal reflection geometry. Other results obtained by our group [20] as well as plasma treating experiments described later in this paper conclusively show that SFG spectra of PS films taken in an external reflection geometry are dominated by the PS-air interface. In the external reflection geometry, it is possible to search for surface in-plane anisotropy of phenyl group orientation by observing the SFG intensity of the aromatic C-H stretch at 3070 cm^{-1} as the sample is rotated about the surface normal as shown in Fig. 1.

The SFG intensity at 3070 cm^{-1} corresponding to the ν_2 vibrational mode as a function of the rotation angle γ for an unrubbed and two rubbed PS films on glass substrates is shown in Fig. 3. The intensity for the unrubbed sample is roughly independent of the rotation angle, whereas the rubbed sample shows a definite anisotropy in SFG intensity with respect to the rotation angle γ.

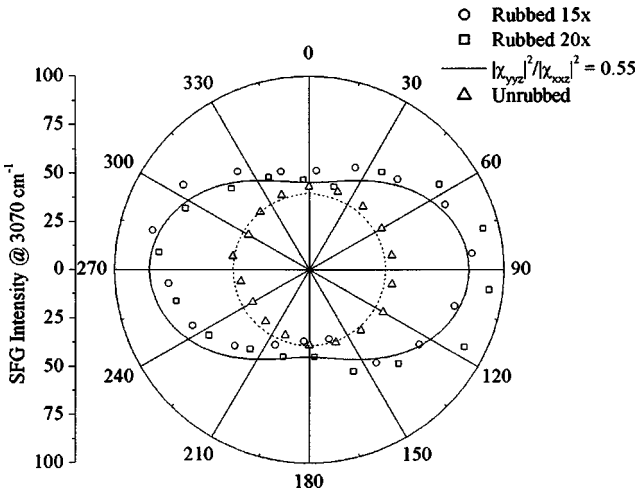

FIG. 3. Plot of the SFG Intensity at 3070 cm^{-1} as a function of rotation angle γ in Fig. 1 for a PS film (520±10)-nm thick before and after rubbing with a velour cloth. The solid line is the SFG intensity calculated using Eqs. (4) and (9) with $|\chi_{yyz}|^2/|\chi_{xxz}|^2 = 0.55$ and $\chi_{xyz}=0$, and the dashed line is a circle of intensity as predicted by Eqs. (4) and (13) for the unrubbed PS film.

The SFG intensity from the ν_2 vibrational mode as a function of the sample orientation can be predicted for different orientations of the phenyl group with respect to the surface. The SFG intensity at $\omega_1+\omega_2$ has the following form [21,22]:

$$I(\omega_1+\omega_2)=\frac{8\pi^3(\omega_1+\omega_2)^2}{c^3 n_1(\omega_1+\omega_2)n_1(\omega_1)n_1(\omega_2)\cos^2\phi'}|\chi_{\mathrm{eff}}|^2 I_1(\omega_1)I_2(\omega_2), \tag{4}$$

where ω_1 and ω_2 are the frequencies of the visible (800 nm) and infrared (3070 cm^{-1}) wavelengths, respectively, I_1 and I_2 are their intensities, n_1 is the refractive index of the first medium, ϕ' is the angle the SFG output beam makes with the surface normal, and χ_{eff} is the effective surface second order susceptibility. The effective surface susceptibility takes into account the magnitude of the electric fields experienced by the molecules at the interface as well as the relationship between the surface polarization vector and the magnitude of the emitted SFG radiation as shown in the following equation [21,22]:

$$\chi_{\mathrm{eff}}=[\bar{\bar{l}}\bar{\bar{L}}(\omega_1+\omega_2)\overline{e}_{\mathrm{SFG}}]\bar{\bar{\chi}}:[\bar{\bar{l}}\bar{\bar{L}}(\omega_1)\overline{e}_1][\bar{\bar{l}}\bar{\bar{L}}(\omega_2)\overline{e}_2], \tag{5}$$

where the diagonal matrices $\bar{\bar{L}}$ and $\bar{\bar{l}}$ describe the Fresnel coefficients and the local field corrections for the incident electric fields; $\overline{e}_1$, $\overline{e}_2$, and $\overline{e}_{\mathrm{SFG}}$ are the unit polarization vectors for the visible, infrared, and SFG beams, respectively; and $\bar{\bar{\chi}}$ is the true surface nonlinear susceptibility.

The true nonlinear surface susceptibility has a resonant, $\langle\bar{\bar{\beta}}\rangle$, and a nonresonant, $\bar{\bar{\chi}}_{\mathrm{NR}}$, component:

$$\bar{\bar{\chi}}=\bar{\bar{\chi}}_{\mathrm{NR}}+N_s\langle\bar{\bar{\beta}}\rangle=N_s\int\bar{\bar{\beta}}(\Omega)f(\Omega)d\Omega. \tag{6}$$

The value Ω represents the set of molecular orientation angles (θ, ψ, ϕ), and $f(\Omega)$ is the orientation probability distribution. The resonant component of the nonlinear susceptibility is the product of the number of molecules on the surface, N_s, and the average of the molecular

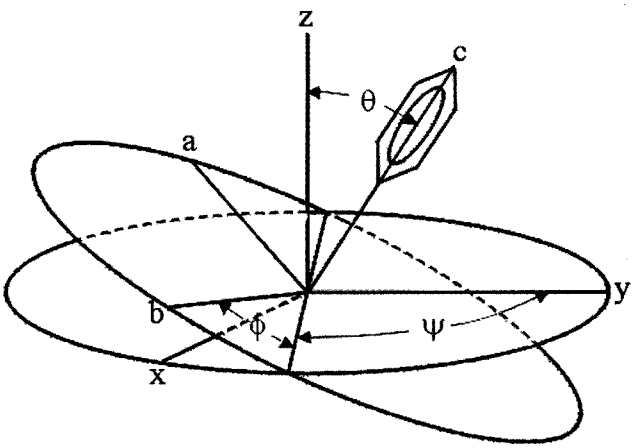

FIG. 4. A diagram showing the relationship between the phenyl group molecular coordinate system (*a*,*b*,*c*) and the laboratory coordinate system (*x*,*y*,*z*) by means of the Euler angles θ, ϕ, and ψ.

hyperpolarizability, $\bar{\bar{\beta}}$. In the *a*, *b*, *c* coordinate system of the phenyl ring as seen in Fig. 4, the hyperpolarizability components for a particular molecular vibration mode, *q*, are the product of the infrared polarizability derivative $\partial\mu_n/\partial q$ and the Raman polarizability tensor element $\partial\alpha_{lm}/\partial q$ of the form [23]:

$$\beta_{lmn} = -\frac{1}{2\omega_q}\frac{\partial\mu_n}{\partial q}\frac{\partial\alpha_{lm}}{\partial q}. \tag{7}$$

The molecular hyperpolarizability tensor components can be estimated by assuming that the additivity of individual C-H bond polarizabilities and dipole moments is valid. If the bond polarizability derivatives for the aromatic C-H stretch as calculated by Whiffen [24] as well as the bond amplitudes used by Duffy *et al.* [23] are used, the hyperpolarizability components for the ν_2 vibrational mode are:

$$\beta_{aac} \approx \beta_{ccc} \gg \beta_{bbc}, \tag{8}$$

where the remaining molecular hyperpolarizability components are all zero.

The elements of the laboratory hyperpolarizability tensor contributing to the SSP SFG intensity can be determined by performing coordinate transformations on Eq. (5). In addition, it is assumed that the surface has symmetry about the *y* axis (the rubbing direction) as well as forward-backward symmetry with respect to the rubbing direction. The assumption of forward-backward symmetry is made because the SFG intensities at $\gamma = 90°$ and 270° are nearly equal; whereas they would be unequal in the presence of significant forward-backward asymmetry. The effective surface hyperpolarizability leading to the ν_2 vibrational contribution to the SSP polarized SFG radiation, $\chi_{\mathrm{eff,SSP}}$, has the following form:

$$\chi_{\mathrm{eff,SSP}} = L_{yy}(\omega_{\mathrm{SFG}})L_{yy}(\omega_1)L_{zz}(\omega_2)[\chi_{xxz}\sin^2\gamma - 2\chi_{xyz}\cos\gamma\sin\gamma + \chi_{yyz}\cos^2\gamma], \tag{9}$$

where L_{yy}, and L_{zz} are the Fresnel coefficients for light polarized parallel to the *y* and *z* axes shown in Fig. 1, and they should incorporate the local field corrections following the procedure described in Refs. [21] and [22].

The orientation of the phenyl ring molecular *a*, *b*, and *c* axes with respect to a surface are shown in Fig. 4. The PS-air interface is parallel to the *x*-*y* plane. The angle ψ, important in describing in-plane orientation, is the direction of the projection of the phenyl *c* axis into the plane of the surface where an angle $\psi = 90°$ means the phenyl *c* axis is tilted by an angle θ towards the *y* axis. The angle ϕ represents the rotation of the phenyl group about the bond connecting it to the PS backbone. When $\phi = 0°$, the plane of the phenyl group is perpendicular to the plane of the surface. The relationships between the laboratory hyperpolarizability coefficients appearing in Eq. (9) and the significant terms of the molecular hyperpolarizability tensor have the following forms (where *r* is the ratio of β_{aac}/β_{ccc}):

$$\chi_{xxz} = \beta_{ccc}[\langle\cos^2\psi\rangle\{\langle\cos^3\theta\rangle[r\langle\cos^2\phi\rangle - 1] + \langle\cos\theta\rangle[1 - r(1 - \langle\cos^2\phi\rangle)]\} + r\langle\cos\theta\rangle[1 - \langle\cos^2\phi\rangle]], \tag{10}$$

$$\chi_{yyz} = \beta_{ccc}[\langle\cos^2\psi\rangle\{-\langle\cos^3\theta\rangle[r\langle\cos^2\phi\rangle - 1] - \langle\cos\theta\rangle[1 - r(1 - \langle\cos^2\phi\rangle)]\} + \langle\cos^3\theta\rangle[r\langle\cos^2\phi\rangle - 1] + \langle\cos\theta\rangle], \tag{11}$$

$$\chi_{xyz} = -\frac{r}{2}\beta_{ccc}\langle\cos^2\theta\rangle\langle\cos\phi\rangle\langle\sin\phi\rangle(2\langle\cos^3\psi\rangle - 1). \tag{12}$$

The SFG intensity at 3070 cm^{-1} from the rubbed PS samples is anisotropic with respect to the rotation angle γ as seen in Fig. 3. The anisotropy of the SFG intensity expressed as the ratio of the intensity at $\gamma=0°$ to the intensity at $\gamma=90°$ is $|\chi_{yyz}|^2/|\chi_{xxz}|^2$ as seen in Eqs. (4), (5), and (9). This ratio obtained from all of the data at $\gamma=0°$, 180° and $\gamma=90°$, 270° is $(45.1\pm6.0)/(81.8\pm8.7)=0.55\pm0.09$. The same ratio obtained by Oh-e and co-workers for rubbed isotactic PS is 0.63 ± 0.07, in agreement with our results [25]. A plot of the SFG intensity from the ν_2 vibrational mode predicted using $|\chi_{yyz}|^2/|\chi_{xxz}|^2=0.55$ in Eqs. (9) and (4) and assuming $\chi_{xyz}=0$ is shown as a solid line in Fig. 3. The fact that $|\chi_{yyz}|^2/|\chi_{xxz}|^2<1$ indicates that the phenyl *c* axes are predominantly oriented perpendicular to the rubbing direction ($\psi=0°$).

The SSP polarized SFG intensity of the unrubbed PS surface is nearly independent of the orientation angle, γ in Fig. 3. This occurs when the orientation of the phenyl rings becomes isotropic in ψ, as in the following equation for the effective surface hyperpolarizability:

$$\chi_{\mathrm{eff,SSP}}=\tfrac{1}{8}L_{yy}(\omega_1)L_{yy}(\omega_s)L_{zz}(\omega_2)\sin(\phi_1)\{\beta_{ccc}(4\langle\cos\theta\rangle-6\langle\cos^3\theta\rangle)+\beta_{aac}[2\langle\cos^3\theta\rangle(1+\langle\cos^2\phi\rangle)+2\langle\cos\theta\rangle]\}. \tag{13}$$

It can be seen that $\chi_{\mathrm{eff,SSP}}$ becomes independent of γ when all possible angles for ψ become equally probable.

C. Plasma treatment of a rubbed PS surface

As a demonstration of the relative surface sensitivity of the optical retardation and SFG techniques, we performed a simple experiment where a rubbed PS film was exposed to a 5-s Ar plasma treatment in a Harrick PDC-32G plasma cleaner. The plasma treatment of a PS film has been shown to destroy the phenyl groups at the PS-air interface, but not at the hidden PS-substrate interface [15,26]. The external reflection geometry SFG spectrum of a rubbed PS film exposed to the plasma can be seen in Fig. 5(a). The peaks in the spectrum associated with the aromatic C-H stretches (3020–3080 cm^{-1}) are eliminated showing that the surface functionality has been destroyed and that PS SFG spectra obtained in external reflection geometry are sensitive only to the PS-air interface. Retardation measurements on a similarly rubbed and plasma treated sample show that the retardation is not completely destroyed by the plasma treatment as seen in Fig. 5(b). This demonstrates that the SFG measurements are sensitive to a region very close to the surface.

D. Relaxation of a rubbed PS surface upon heating

Having shown that SFG is sensitive to the in-plane orientation of phenyl rings at the rubbed PS-air interface, we can study the relaxation of the orientation of a PS free surface. In this portion of the study, PS films were created on sapphire prism substrates. The prism substrate allows SFG spectra to be taken in an internal reflection geometry that yields an enhancement in the SFG intensity from the PS-air interface when the incident angle is equal to the critical angle for total internal reflection at the PS-air interface (36°) [15]. The films on the prisms are rubbed and mounted on a controlled heating stage with $\gamma=90°$. Inspection of Fig. 3 reveals that at $\gamma=90°$, the SFG intensity should decrease as the surface orientation of the phenyl groups relaxes from the rubbed state to the unrubbed state upon heating. Figure 6 shows the SFG intensity of the ν_2 vibrational mode at 3070 cm^{-1} as a rubbed PS film is heated and then cooled at a rate of 1 K min^{-1}. It is clear that the intensity does decrease as the rubbed film is heated due to surface relaxation. Furthermore, the SFG intensity decreases to ~60% of its initial value after being heated to ~370 K. The magnitude of this drop is consistent with that expected by inspection of Fig. 3 if a rubbed film aligned with $\gamma=90°$ went from the rubbed state to the isotropic, or unrubbed state.

At this point, we would like to address concerns that the SFG intensity changes observed are due to shifts in the critical angle for total internal reflection caused by temperature induced changes in the refractive indices of PS or sapphire. Equations (4) and (5) show that the SFG intensity is proportional to the Fresnel coefficients, which are in turn sensitive to the incident angles, ϕ_1, ϕ_2, and ϕ_3, relative to the critical angles for total internal reflection. Snell's law for a three layer system [27] states that $n_1\sin\phi_1=n_2\sin\phi_2=n_3\sin\phi_3$, where materials 1, 2, and 3 are sapphire, PS, and air, respectively. The observed critical angle for total internal reflection at the PS-air interface occurs when $\phi_3=90°$. The experimental PS-air critical angle occurs when $\phi_1=\sin^{-1}(n_3/n_1)$ and is independent of the refractive index of PS. This means any changes in the refractive index of rubbed PS due to relaxation of birefringence will have no effect on the observed position of the critical angle. The critical angle is, however, affected by changes in the refractive index of sapphire, assuming the refractive index of air does not change significantly over the temperature range of the experiment. Therefore, changes in the critical angle with temperature caused by changes in the sapphire prism's refractive index are expected to be reversible in temperature. The SFG intensity seen in Fig. 6 does not return upon cooling, indicating that any shifts in the PS-air critical angle have no effect on the changes in SFG intensity seen upon heating a rubbed PS sample.

In order to compare the surface relaxation results obtained with SFG to those obtained from birefringence, it is necessary to take an in-depth look at what type of orientation the two techniques are probing. The relationship between birefringence and orientation in uniaxially stretched polymer materials is described by the Hermans orientation function [28]

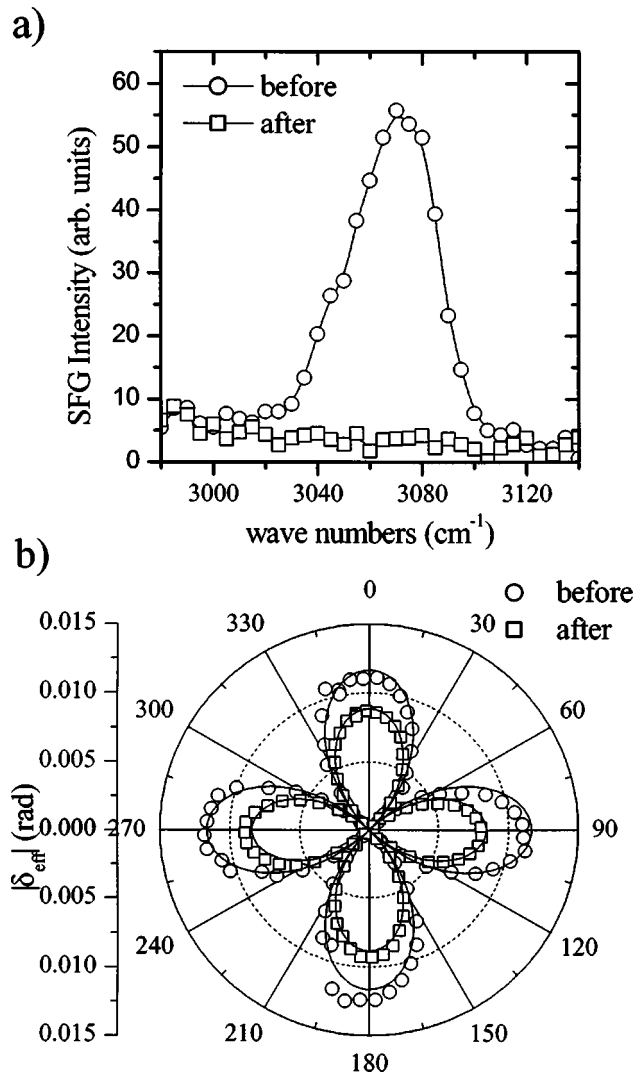

FIG. 5. (a) SFG spectrum of the PS-air interface before and after a 5-s Ar plasma treatment. The disappearance of the broad peak centered at 3070 cm^{-1} indicates the elimination of the phenyl moiety from the PS-air interface. (b) The effective retardation, δ_{eff}, of a PS film 200-nm thick before and after a 5-s Ar plasma treatment. A slight decrease in the retardation magnitude in the plasma treated sample is due to the surface alteration effects of the plasma.

$$\Delta n = \Delta n_{\text{int}} \frac{3\langle \cos^2 \eta \rangle - 1}{2}, \tag{14}$$

where η is the average angle a polymer repeat unit backbone makes with the drawing direction and Δn_{int} is the intrinsic birefringence of the polymer repeat unit. The SFG intensity, on the other hand, is proportional to $|a\langle \cos^2 \psi \rangle + b|^2$ as seen in Eq. (10), where the coefficients a and b are dependent on the Fresnel coefficients, the molecular hyperpolarizability tensor elements, and the molecular orientation angles θ and ϕ. If the square root of the SFG intensity during relaxation, $\sqrt{I_{\text{SSP}}}$, is subtracted from the square root of the SFG intensity after relaxation is complete, $\sqrt{I_{\text{SSP},\infty}}$, and the angles θ and ϕ are assumed to be constant, the following expression is obtained:

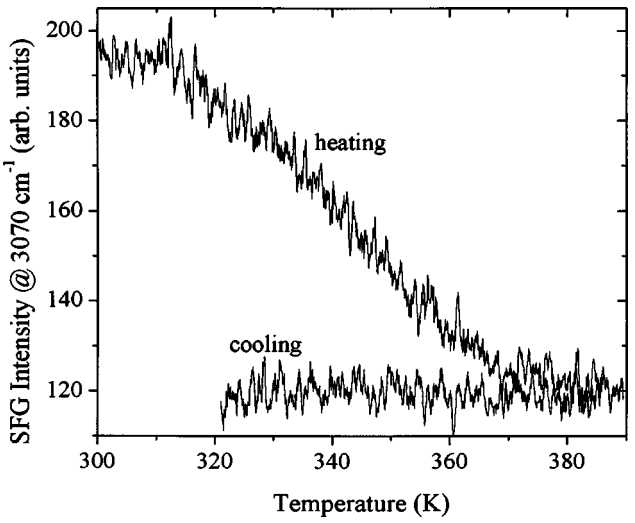

FIG. 6. Relaxation of the SFG intensity at 3070 cm^{-1} in a rubbed PS film (520±10)-nm thick mounted with $\gamma = 90°$ and heated at a constant rate of 1 K min^{-1}. Also included is the SFG intensity at 3070 cm^{-1} as the same film is cooled from 390 to 320 K at a rate of 1 K min^{-1}.

$$\sqrt{I_{\text{SSP}}} - \sqrt{I_{\text{SSP},\infty}} \propto a(\langle \cos^2 \psi \rangle - \tfrac{1}{2}). \tag{15}$$

The expression in Eq. (15) represents a way to present the SFG relaxation data to obtain an order parameter in terms of $\langle \cos^2 \psi \rangle$. Assuming that the PS backbone segments lie in the plane of the surface and the PS phenyl side groups are oriented roughly perpendicular to the polymer backbone, the angle ψ represents the surface or two-dimensional analog of the angle η. In essence, the SFG order parameter as presented in Eq. (15) can be directly compared to the order parameter obtained from birefringence (optical retardation) measurements.

In Fig. 7(a) are the relaxation of birefringence data for a lightly rubbed thick (10 μm) PS film and a highly rubbed thick PS film obtained in previous studies [6,7]. As mentioned earlier, the orientation in a lightly rubbed film does not penetrate as deep into the film as the orientation in a highly rubbed film. We have estimated the penetration depth of the orientation, d_{eff}, to be 7 and 28 nm for the lightly rubbed and highly rubbed thick films, respectively [6,7]. The relaxation behavior exhibited for these films should therefore probe the average relaxation dynamics in the top 7 and 28 nm of the lightly and highly rubbed thick films, respectively. Figure 7(b) shows the results of a surface relaxation measurement with the SFG intensity presented as in Eq. (15). By comparing the data in Figs. 7(a) and 7(b), it can be seen that the surface relaxation appears very similar to that of the lightly rubbed thick PS film.

The retardation and SFG relaxation data can be fit using a constant heating rate relaxation model previously developed [6,7] and seen in Eq. (16). The model assumes a Kohlrausch-William-Watts (KWW) [29] stretched exponential time dependence for the retardation, δ with a stretching exponent β_{KWW}, temperature dependent relaxation time τ, for experiments performed at a constant linear heating rate of A,

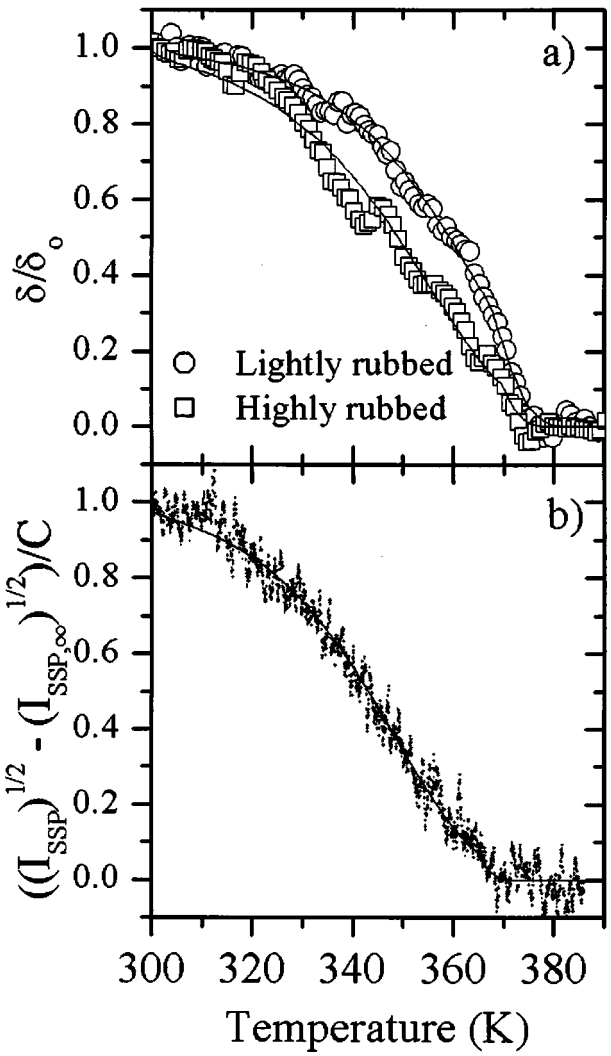

FIG. 7. (a) Relaxation of retardation for a lightly rubbed and a highly rubbed PS film (10-μm thick) heated at a rate of 1 K min^{-1} [6,7]. (b) Relaxation of SFG intensity modified as per Eq. (15) and as described in text. All relaxation curves are normalized to their initial values before the onset of heating. The solid lines represent the fits to the data obtained using the relaxation model shown in Eqs. (16) and (17).

$$\delta(T)=\delta_o \exp\left[-\int_{T_o}^{T}\frac{\beta_{\mathrm{KWW}}(T-T_o)^{\beta_{\mathrm{KWW}}-1}}{[A\tau(T)]^{\beta_{\mathrm{KWW}}}}dT\right]. \quad (16)$$

The relaxation time is assumed to follow an Arrhenius temperature dependence below T_g and a Williams-Landel-Ferry (WLF) temperature dependence [30] above T_g as seen in Eq. (17),

$$\tau(T)=\begin{cases}\tau(T_g)\exp\left[-\dfrac{\Delta E}{R}\left(\dfrac{1}{T}-\dfrac{1}{T_g}\right)\right], & T<T_g\\ \tau(T_g)\times 10^{-c_1(T-T_g)/(c_2+T-T_g)}, & T\geqslant T_g\end{cases}. \quad (17)$$

The WLF parameters c_1 and c_2 are 13.7 and 50.0 K, respectively. The relaxation time at T_g, $\tau(T_g)$, is assumed to be 5 s based on experimental measurements of relaxation times in PS near T_g [31–36]. We have also conducted isothermal birefringence relaxation measurements below T_g and the results are in good agreement with those obtained using a constant heating rate of 1 K min^{-1} [37]. This indicates that a KWW equation along with Arrhenius temperature dependence is a good model for relaxation below T_g.

The relaxation curves in Fig. 7 as well as other data presented previously [6,7] can be fit with Eqs. (16) and (17) to obtain useful relaxation parameters such as the stretching exponent β_{KWW}, the activation energy ΔE, and the glass transition temperature T_g. In the analysis presented originally, the retardation relaxation curves from 10-μm-thick PS films rubbed to different strengths were fit with the activation energy ΔE and β_{KWW} fixed at 205 kJ mol^{-1} and 0.36, respectively [6,7]. This procedure was adopted because similar measurements on films of varying thicknesses indicated that ΔE and β_{KWW} did not vary with film thickness. A better fit of the data was obtained by floating all three parameters, ΔE, β_{KWW}, and T_g and the results are summarized in Fig. 8. The results indicate that the activation energy and relaxation exponent of the near surface region are actually different than those of the bulk. The relaxation parameters are plotted as a function of the initial retardation as well as the estimated depth of orientation, d_{eff}. The SFG relaxation data of this study are represented as $d_{\mathrm{eff}}=0$ because it is a measure of the surface dynamics.

It can clearly be seen in Fig. 8(a) that the activation energy ΔE of the surface is lower than that of the bulk. The most highly rubbed PS thick film relaxation data presented in Fig. 8 are indicative of bulk relaxation dynamics. In addition, the stretching exponent β_{KWW} of surface is larger than that in the bulk, indicating a narrower distribution of relaxation times at the surface relative to the bulk [Fig. 8(b)]. The stretching exponent can be used to account for a distribution of relaxation times where a decreasing β_{KWW} value represents a broader distribution of relaxation times. Both the lower activation energy and larger β_{KWW} value of the surface can be rationalized by the existence of a relatively free environment at the surface with less hindrance to relaxation processes.

In contrast to the generally held belief, the SFG relaxation data indicate that the surface does not have a significantly lower glass transition temperature than the bulk [T_g ($d_{\mathrm{eff}}=0$)$=365.0\pm 2.6$ K and T_g ($d_{\mathrm{eff}}=31.9$ nm)$=366.1\pm 0.9$ K]. This difference in T_g is not as large as 57 K as seen in positron annihilation measurements [13], nor does it indicate the surface has a T_g of 305 K as expected from theoretical models applied to supported thin film data [38]. The glass transition temperature is defined here as the temperature when $\tau=5$ s. The enhanced mobility believed to exist at the surface does actually appear below T_g as demonstrated in Fig. 9. A lower surface activation energy naturally causes surface relaxation times at any temperature below T_g to be lower than those of bulk PS. Though the mobility of the surface is enhanced, it is not a liquid, where our current definition of a liquid would require $\tau<5$ s. Little comment can be made, unfortunately, on the temperature dependence of the surface relaxation times above T_g because they cannot be adequately captured using the current experimental setup.

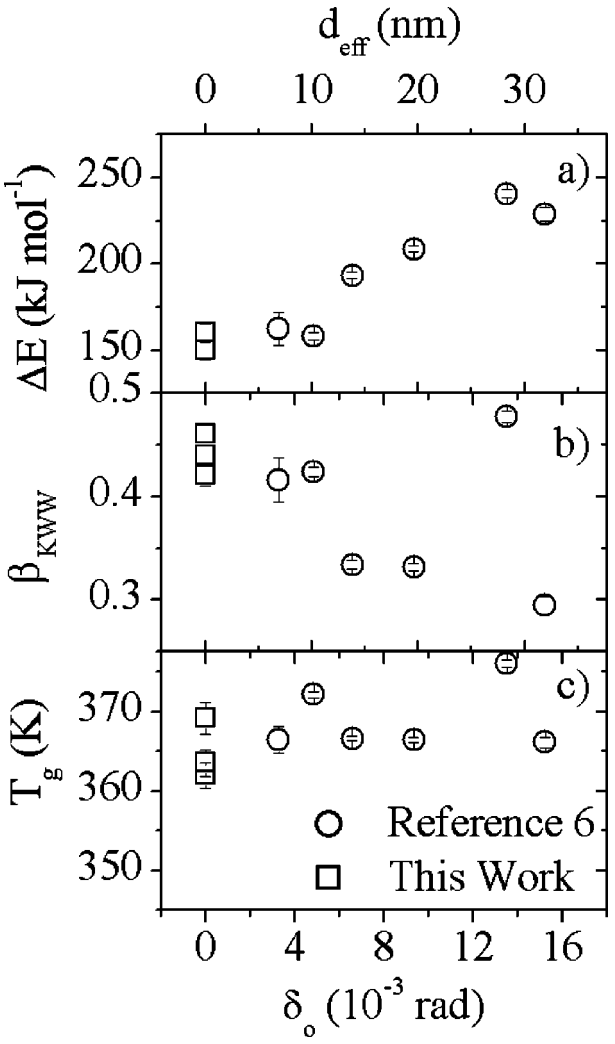

FIG. 8. Plot of (a) activation energy ΔE, (b) stretching exponent β_{KWW}, and (c) glass transition temperature T_g, as a function of rubbing strength quantified as the initial retardation δ_o in thick (10 μm) PS films. The top horizontal axes represent an estimation of the effective rubbing depth d_{eff} obtained for each rubbing strength. The surface sensitive results of this work are represented as having an effective depth of zero ($d_{\mathrm{eff}}=0$).

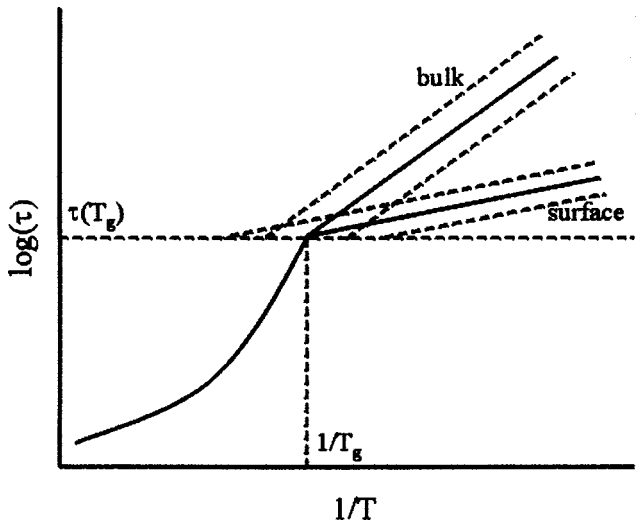

FIG. 9. Conceptual plot illustrating the differences in relaxation times obtained for bulk and surface relaxation times in PS. The solid lines indicate the average relaxation time and the dashed lines are indicative of the breadth of the relaxation time distribution as determined from β_{KWW}. Experimentally, the activation energy of the surface [$\Delta E=153\pm3$ kJ mol^{-1}] was found to be lower than that of the bulk [$\Delta E=206\pm20$ kJ mol^{-1}], and the stretching exponent of the surface ($\beta_{\mathrm{KWW}}=0.44\pm0.01$) was found to be higher than that of the bulk ($\beta_{\mathrm{KWW}}=0.37\pm0.06$). The surface relaxation dynamics above T_g could not be characterized in this study.

Figure 9 also illustrates the dangers of attempting to infer changes in T_g for polymer surfaces and for thin polymer films from dynamic or diffusion experiments performed at a single temperature. The observation of faster relaxation times or faster diffusion in a polymer film or near a polymer surface does not necessarily indicate that the film has a lower glass transition temperature. It may, rather, indicate that the temperature dependence of the diffusion or relaxation processes have changed with film thickness.

Furthermore, the temperature dependence of dynamic mechanical properties measured at a single frequency cannot necessarily provide correct information on surface T_g. In these types of experiments, surface T_g is assumed to be the temperature where the surface mechanical properties change from being elastic to rubbery or liquidlike. From Fig. 9, it can be seen that the frequency of the measurement should affect the "T_g" determined in this manner. For example, measurements performed at higher frequencies should yield values for "T_g" that are higher than comparable measurements performed at lower frequencies. Furthermore, the difference in the surface and bulk "T_g" as determined by dynamic measurements of this type should increase with decreasing measurement frequency.

This is exactly the behavior that has been seen using atomic force microscopy to study surface mechanical properties. Dinelli *et al.* find that the surface T_g determined by measuring the temperature dependence of the frictional force between an atomic force microscope (AFM) tip sliding at a constant velocity and a PS surface increases with increasing sliding velocity (~frequency) [39]. Kajiyama *et al.* also showed that the surface frictional properties at different sliding rates and temperatures appeared to follow time temperature superposition, and the shift factor appeared to follow an Arrhenius temperature dependence [40]. A lower surface activation energy also resolves the discrepancy between Refs. [9] and [8]. Kajiyama *et al.* find that the PS surface T_g is lower than the bulk, especially at lower molecular weights, as determined using an AFM tip sliding velocity of 1 μm s^{-1} [9]. Ge *et al.*, on the other hand, use an oscillatory sliding motion for the AFM tip with an amplitude of 3 nm and a frequency of 1400 Hz [8]. This correlates to a peak sliding velocity of 26 μm s^{-1}, which may explain why they find that the surface T_g is not lower than bulk T_g regardless of the PS molecular weight [8].

The estimated size of the surface region of lower activation energy also helps to explain the discrepancy between previous NEXAFS results [10,11]. Liu *et al.* used a

NEXAFS technique and found that the top 1 nm of a rubbed PS film does not relax more quickly than the top 10 nm [10]. Wallace *et al.*, on the other hand find that the top 2 nm of a uniaxially drawn PS film relax more quickly than the top 200 nm [11]. The results shown in Fig. 8 clearly show little difference between the surface relaxation parameters ($d_{\mathrm{eff}}=0$) and the relaxation parameters obtained for the top 10 nm, thereby explaining the discrepancy between the results of Liu *et al.* and Wallace *et al.*

Finally, some comment should be made on the relationship between the length scales of the surface region with enhanced mobility and the length scale where thin film T_g begins to significantly drop. The region of enhanced mobility near the surface of PS appears to be roughly ~12-nm thick as seen in Fig. 8. Similarly, significant drop in PS film T_g occurs when PS film thickness drops below ~30 nm [1–3,6,7]. Exactly how this surface region of reduced activation energy later manifests itself as a decreasing T_g with decreasing film thickness is not entirely clear, but the reduction in film T_g does not apparently occur until the entire volume of the film is composed of similarly affected surface regions.

IV. CONCLUSIONS

Many experiments [1–7] and computer simulations [41–43] have indicated the existence of a surface layer with enhanced mobility at the free surface of a glassy polymer, and the measurements presented here are conclusive evidence for its existence below T_g. This layer, estimated to be ~12-nm thick, is well characterized as having an lower activation energy and a narrower distribution of relaxation times relative to those of bulk PS.

ACKNOWLEDGMENTS

We gratefully acknowledge funding from NSF (DMR9984996) (A.D.) and Lord Corporation (A.S.) for this work. We also thank Professor Satyendra Kumar for the loan of the PEM for the birefringence measurements.

[1] J. L. Keddie, R. A. L. Jones, and R. A. Cory, Europhys. Lett. **27**, 59 (1994).
[2] S. Kawana and R. A. L. Jones, Phys. Rev. E **63**, 021501 (2001).
[3] J. A. Forrest and K. Dalnoki-Veress, Adv. Colloid Interface Sci. **94**, 167 (2001).
[4] K. Fukao and Y. Miyamoto, Europhys. Lett. **46**, 649 (1999).
[5] K. Fukao and Y. Miyamoto, Phys. Rev. E **61**, 1743 (2000).
[6] A. D. Schwab, D. M. G. Agra, J.-H. Kim, S. Kumar, and A. Dhinojwala, Macromolecules **33**, 4903 (2000).
[7] D. M. G. Agra, A. D. Schwab, J.-H. Kim, S. Kumar, and A. Dhinojwala, Europhys. Lett. **51**, 655 (2000).
[8] S. Ge, Y. Pu, W. Zhang, M. Rafailovich, J. Sokolov, C. Buenviage, R. Buckmaster, and R. M. Overney, Phys. Rev. Lett. **85**, 2340 (2000).
[9] T. Kajiyama, K. Tanaka, N. Satomi, and A. Takahara, Sci. Technol. Adv. Mater. **1**, 31 (2000).
[10] Y. Liu, T. P. Russell, M. G. Samant, J. Stohr, H. R. Brown, A. Cossy-Favre, and J. Diaz, Macromolecules **30**, 7768 (1997).
[11] W. E. Wallace, D. A. Fischer, K. Efimenko, W.-L. Wu, and J. Genzer, Macromolecules **34**, 5081 (2001).
[12] L. Xie, G. B. DeMaggio, W. E. Frieze, J. DeVries, D. W. Gidley, H. A. Hristov, and A. F. Yee, Phys. Rev. Lett. **74**, 4947 (1995).
[13] Y. C. Jean, R. Zhang, H. Cao, J.-P. Yuan, C.-M. Huang, B. Nielsen, and P. Asoka-Kumar, Phys. Rev. B **56**, R8459 (1997).
[14] T. C. Oakberg, *Linear Birefringence and Optical Rotation* (Hinds Instruments Inc., 1993).
[15] K. S. Gautam, A. D. Schwab, A. Dhinojwala, D. Zhang, S. M. Dougal, and M. S. Yeganeh, Phys. Rev. Lett. **85**, 3854 (2000).
[16] R. M. A. Azzam and N. M. Bashara, *Ellipsometry and Polaraized Light* (Elsevier, Amsterdam, 1987).
[17] N. A. J. M. Van Aerle, M. Barmentlo, and R. W. J. Hollering, J. Appl. Phys. **74**, 3111 (1993).
[18] L.-H. Wang, C. L. Choy, and R. S. Porter, J. Polym. Sci., Polym. Phys. Ed. **20**, 633 (1982).
[19] K. A. Briggman, J. C. Stephenson, W. E. Wallace, and L. J. Richter, J. Phys. Chem. B **105**, 2785 (2001).
[20] K. S. Gautam and A. Dhinojwala, Phys. Rev. Lett. **88**, 145501 (2002).
[21] X. Wei, X. Zhuang, S.-C. Hong, T. Goto, and Y. R. Shen, Phys. Rev. Lett. **82**, 4256 (1999).
[22] X. Wei, S.-C. Hong, X. Zhuang, T. Goto, and Y. R. Shen, Phys. Rev. E **62**, 5160 (2000).
[23] D. C. Duffy, P. B. Davies, and C. D. Bain, J. Phys. Chem. **99**, 15 241 (1995).
[24] W. H. Whiffen, Proc. Phys. Soc., London, Sect. A **69**, 375 (1956).
[25] M. Oh-e, S.-C. Hong, and Y. R. Shen, Appl. Phys. Lett. **80**, 784 (2002).
[26] D. Zhang, S. M. Dougal, and M. S. Yeganeh, Langmuir **16**, 4528 (2000).
[27] M. Born and E. Wolf, *Principles of Optics*, 7th ed. (Cambridge University Press, Cambridge, 1999).
[28] I. M. Ward, *Structure and Properties of Oriented Polymers* (Wiley, New York, 1975).
[29] G. Williams and D. C. Watts, Trans. Faraday Soc. **66**, 80 (1971).
[30] M. L. Williams, R. F. Landel, and J. D. Ferry, J. Am. Chem. Soc. **77**, 3701 (1955).
[31] S. Saito and T. Nakajima, J. Appl. Polym. Sci. **2**, 93 (1959).
[32] A. Dhinojwala, G. K. Wong, and J. M. Torkelson, J. Chem. Phys. **100**, 6046 (1994).
[33] T. Inoue, M. T. Cicerone, and M. D. Ediger, Macromolecules **28**, 3425 (1995).
[34] V. S. Kastner, E. Schlosser, and G. Pohl, Kolloid Z. Z. Polym. **192**, 21 (1963).
[35] C. P. Lindsey, G. D. Patterson, and J. R. Stevens, J. Polym. Sci., Polym. Phys. Ed. **17**, 1547 (1979).
[36] H. Lee, A. M. Jamieson, and R. Simha, Macromolecules **12**, 329 (1979).
[37] A. D. Schwab, B. Acharya, S. Kumar, and A. Dhinojwala,

Mod. Phys. Lett. **16**, 415 (2002).
[38] J. A. Forrest and J. Mattsson, Phys. Rev. E **61**, R53 (2000).
[39] F. Dinelli, C. Buenviaje, and R. M. Overney, J. Chem. Phys. **113**, 2043 (2000).
[40] T. Kajiyama, K. Tanaka, N. Satomi, and A. Takahara, Macromolecules **31**, 5150 (1998).
[41] K. F. Mansfield and D. N. Theodorou, Macromolecules **24**, 6283 (1991).
[42] P. Doruker and W. L. Mattice, Macromolecules **32**, 194 (1999).
[43] T. S. Jain and J. J. de Pablo, Macromolecules **35**, 2167 (2002).